Title
Thermodynamics of block copolymers with and without salt.

Journal
The journal of physical chemistry. B, 118(1)

ISSN
1520-6106

Authors
Teran, Alexander A
Balsara, Nitash P

Publication Date
2014

DOI
10.1021/jp408079z

Peer reviewed

THE JOURNAL OF PHYSICAL CHEMISTRY B

Feature Article

pubs.acs.org/JPCB

Thermodynamics of Block Copolymers with and without Salt

Alexander A. Teran[†,‡] and Nitash P. Balsara*[,†,‡,§]

[†]Environmental Energy Technologies Division, Lawrence Berkeley National Laboratory, Berkeley, California 94720, United States

[‡]Department of Chemical & Biomolecular Engineering, University of California, Berkeley, California 94720, United States

[§]Materials Sciences Division, Lawrence Berkeley National Laboratory, Berkeley, California 94720, United States

Supporting Information

ABSTRACT: Ion-containing block copolymers are of interest for applications such as electrolytes in rechargeable lithium batteries. The addition of salt to these materials is necessary to make them conductive; however, even small amounts of salt can have significant effects on the phase behavior of these materials and consequently on their ion-transport and mechanical properties. As a result, the effect of salt addition on block copolymer thermodynamics has been the subject of significant interest over the past decade. This feature article describes a comprehensive study of the thermodynamics of block copolymer/salt mixtures over a wide range of molecular weights, compositions, salt concentrations, and temperatures. The Flory–Huggins interaction parameter was determined by fitting small-angle X-ray scattering data of disordered systems to predictions based on the random phase approximation. Experiments on neat block copolymers revealed that the Flory–Huggins parameter is a strong function of chain length. Experiments on block copolymer/salt mixtures revealed a highly nonlinear dependence of the Flory–Huggins parameter on salt concentration. These findings are a significant departure from previous results and indicate the need for improved theories for describing thermodynamic interactions in neat and salt-containing block copolymers.

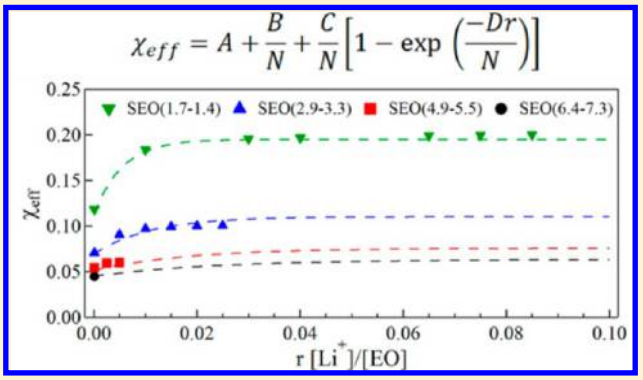

INTRODUCTION

Block copolymers are a class of materials in which a chain of identical molecules is covalently bonded to a chain of a different molecule. The most basic version of a block copolymer is a linear diblock copolymer, shown in Figure 1, in which two chemically distinct chains, or blocks, are linked end-to-end. Using this strategy, one can create materials with many blocks bonded together into as many different molecular architectures as current synthetic strategies will allow. This work focuses exclusively on nearly monodisperse diblock copolymers. The classic battle between entropy and enthalpy, coupled with the geometric constraints on phase separation, causes these materials to self-assemble into nanostructured morphologies with length scales on the order of 5–100 nm. These ordered morphologies include stacked lamellae (LAM), bicontinuous gyroids (GYR), and hexagonally packed cylinders (HEX) among others. At sufficiently high temperature, entropy dominates, resulting in the formation of a disordered phase (DIS) in which the two blocks are homogeneously mixed; the nature of concentration fluctuations in the disordered phase has been studied in considerable detail.[1] This self-assembly, or lack thereof, is controlled by the volume fraction of one component f and the degree of segregation χN, where N is the overall degree of polymerization and χ is the Flory–Huggins interaction parameter, which is a measure of thermodynamic compatibility between the blocks. By tuning these parameters appropriately, it is possible to obtain nanostructured materials that combine the material properties of the constituent blocks. This has led researchers to use block copolymers as solid membranes for selective transport of various species, typically with one transporting block and one structural block. Of particular interest in recent years are block copolymers with added ions that selectively dissolve in one block for applications such as solid-state electrolytes in rechargeable lithium batteries. Such materials can offer high conductivity, stable electrochemical characteristics, and excellent mechanical properties. One commonly studied system is polystyrene-*b*-poly(ethylene oxide) (SEO).[2,3] Polyethylene oxide (PEO) has been studied for several decades as a polymer electrolyte due to its ability to dissolve alkali salts,[4−6] and polystyrene (PS) is a mechanically rigid polymer.

The thermodynamic properties of block copolymers with and without added salt have been the subject of several investigations.[7−15] Most of the work in this field is built on the assumption that the interaction parameter of the neat copolymer χ_0 is independent of N despite comprehensive studies by Mori et al.[7] and Lin et al.[8] that demonstrate that χ_0

Received: August 12, 2013
Revised: October 17, 2013
Published: November 15, 2013

   dx.doi.org/10.1021/jp408079z | J. Phys. Chem. B 2014, 118, 4–17

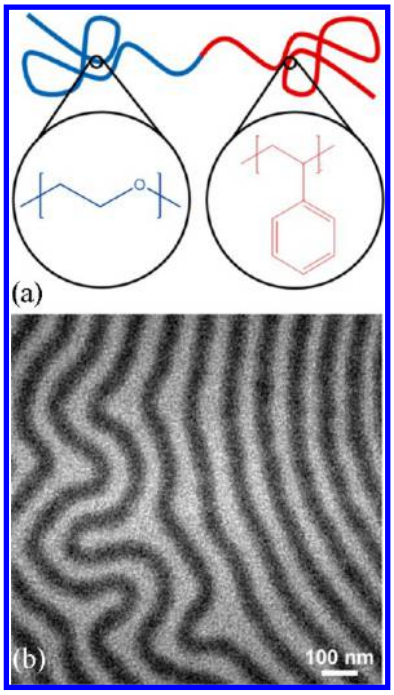

Figure 1. (a) Schematic of an SEO diblock copolymer. (b) TEM micrograph of lamellar SEO(74–98) with $LiPF_6$ at r = 0.17 [Li^+]/[EO] spun-cast from *N*-methylpyrrolidone. The substrate was holey silicon nitride, and the image is of a portion of free-standing film over one of those holes.

between PS and polyisoprene (PI) in symmetric block copolymers decreases with increasing N.

The addition of salt to such copolymers, which is necessary to imbue them with ionic conductivity, can have a substantial effect on their material properties. Even small amounts of salt can change the phase behavior of the copolymer. Current work suggests that this is due to an increase in the effective interaction parameter χ_{eff} between the structural block and the salt-containing block.[16] Both the ion transport and the mechanical properties of these materials are affected by the morphology and degree of segregation. It is therefore of great practical interest to understand this effect. All of the previous theoretical and experimental work, including work from our laboratory, suggests that χ_{eff} increases linearly with increasing salt concentration. The exception to this is the work of Huang et al.[9] who showed that the relationship between χ_{eff} and salt concentration is distinctly nonlinear, with a steep slope at low salt concentrations and plateau-like behavior at high salt concentration. The theoretical work of Nakamura and Wang indicates that nonlinear χ_{eff} versus salt concentration data are a signature of incomplete dissociation.[14] In the limit of complete dissociation, their theory predicts a strong linear increase in the dependence of χ_{eff} on salt concentration.

The purpose of this study is to present a comprehensive study of block copolymer thermodynamics over a wide range of block copolymer molecular weights, compositions, salt concentrations, and temperatures. The value of χ_{eff} for a series of SEO copolymers with lithium bis(trifluoromethanesulfone)-imide (LiTFSI) salt was measured directly by fitting random phase approximation (RPA) theory to small-angle X-ray scattering (SAXS) profiles of disordered SEO/LiTFSI mixtures. Our data overwhelmingly reaffirms that χ_0 is a strong function of N; ignoring this effect has a profound impact on the interpretation of thermodynamic data from salty samples. In particular, complex nonlinear dependencies of χ_{eff} on salt concentration are presented, and we even show data wherein the addition of salt leads to a decrease in χ_{eff}.

EXPERIMENTAL SECTION

Materials. The SEO copolymers in this study were synthesized, purified, and characterized using methods described in refs 17 and 18. Additionally, the copolymers were passed through a column of neutral alumina and 0.2 μm cellulose filters until the residual reaction byproducts were no longer detectable using ^{1}H NMR spectroscopy. The polymers used in this study are called SEO(xx–yy), where xx and yy are the number-averaged molecular weights of the PS, M_{PS}, and poly(ethylene oxide) (PEO), M_{PEO}, blocks in kg mol^{-1}, respectively. The volume fraction of the copolymers is given by

$$\phi_{EO} = \frac{\nu_{EO}}{\nu_{EO} + \frac{M_{PS}M_{EO}}{M_S M_{PEO}}\nu_S} \quad (1)$$

where ν_{EO} and ν_S are the molar volumes of ethylene oxide monomer units and styrene monomer units, respectively, and M_S and M_{EO} are the molar masses of styrene (104.15 g mol^{-1}) and ethylene oxide (44.05 g mol^{-1}), respectively. Molar volumes were calculated by

$$\nu = M/\rho \quad (2)$$

In this work, $\rho_{PEO} = 1.139 - 7.31 \times 10^{-4} \times T$ and $\rho_{PS} = 1.0865 - 6.19 \times 10^{-4} \times T + 1.36 \times 10^{-7} \times T^2$ for the densities of the PEO block and the PS block, respectively.[19] The overall degree of polymerization was calculated by

$$N = N_{PEO} + N_{PS} \quad (3)$$

where

$$N_i(T) = \frac{M_i}{\rho_i(T) N_{avg} \nu_{ref}} \quad (4)$$

and ν_{ref} was fixed at 0.1 nm^3. A list of the polymer characteristics, including the polydispersity index of the block

Table 1. Characteristics of the Copolymers in This Study

polymer	M_{PS}	M_{PEO} kg mol^{-1}	M	N_{PS}	N_{PEO} at 140 °C	N	PDI	ϕ_{EO}	morphology	T_{ODT} °C
SEO(1.9–0.8)	1.9	0.8	2.7	30	12	42	1.05	0.29	DIS	
SEO(1.4–1.6)	1.4	1.6	3.0	22	24	46	1.03	0.52	DIS	
SEO(1.7–1.4)	1.7	1.4	3.1	27	21	48	1.05	0.44	DIS	
SEO(2.9–3.3)	2.9	3.3	6.2	46	50	96	1.05	0.52	DIS	
SEO(4.9–5.5)	4.9	5.5	10.4	78	83	161	1.04	0.52	DIS	
SEO(6.4–7.3)	6.4	7.3	13.7	101	111	212	1.04	0.52	LAM → DIS	107.5

dx.doi.org/10.1021/jp408079z | J. Phys. Chem. B 2014, 118, 4–17

copolymer PDI, can be found in Table 1. The neat copolymers are completely transparent and colorless.

Electrolyte Preparation. The salt-containing copolymers were prepared using methods described in ref 20. Because of the hygroscopic nature of the salt, argon gloveboxes (MBraun) with oxygen and water below parts per million levels were used for all sample preparation. The salt concentration in our copolymer was quantified by r the molar ratio of lithium ions to ethylene oxide (EO) moieties. The number of EO units in the copolymer is calculated from the molecular weight of the PEO block without correcting for end groups. We assume that the salt resides exclusively in the PEO domain[21] and determine the volume fraction of the new PEO/salt microphase by

$$\phi_{\mathrm{EO/salt}}(r) = \frac{v_{\mathrm{EO}} + r v_{\mathrm{LiTFSI}}}{v_{\mathrm{EO}} + r v_{\mathrm{LiTFSI}} + \frac{M_{\mathrm{PS}} M_{\mathrm{EO}}}{M_{\mathrm{S}} M_{\mathrm{PEO}}} v_{\mathrm{S}}} \quad (5)$$

where ν_{LiTFSI} is the molar volume of LiTFSI, calculated using a density of $\rho_{\mathrm{LiTFSI}} = 2.023$ g cm^{-3} and a molar mass of $M_{\mathrm{LiTFSI}} = 287.09$ g mol^{-1}. A full list of samples used in this study can be found in Table 2.

Small Angle X-ray Scattering. SAXS samples were prepared by pressing/melting the polymer into aluminum spacers and annealing them at 90 °C for at least 24 h. The samples were sealed with Kapton windows in custom-designed airtight holders. Samples were mounted in a custom-built 8-sample heating stage and annealed at each temperature for 20 min before taking measurements. Actual sample thicknesses were measured after experiments were completed and ranged from about 2 to 4 mm.

SAXS measurements were performed at beamline 7.3.3 at the Advanced Light Source (ALS) at Lawrence Berkeley National Laboratory. Silver behenate was used to determine the beam center and sample-to-detector distance. The scattered intensity was corrected for beam transmission, empty cell scattering, as well as for unavoidable air gaps in the system. Glassy carbon was used to determine the scaling calibration to obtain the absolute intensity scattering. Two-dimensional scattering patterns were integrated azimuthally using the Nika program for IGOR Pro to produce one-dimensional (1D) scattering profiles.[22]

RESULTS AND DISCUSSION

Pure Copolymers. Figure 2 shows the scattering intensity as a function of wave vector q of four nearly symmetric SEO copolymers in the neat state at 110 °C. All four polymers are in the disordered state, indicated by the single broad scattering peak. The arrows indicate the location of the primary scattering peak q^*. The domain spacing d of the copolymers can be determined by the equation

$$d = 2\pi/q^* \quad (6)$$

The location of q^* shifts to higher values as the molecular weight of the copolymers decreases, representing a corresponding decrease in the characteristic length scale of the copolymer. The intensity of the scattering also decreases as the molecular weight decreases. The intensity of SEO(1.7−1.4) in Figure 2d is so low that at first glance it is difficult to locate the primary scattering peak; the inset shows the primary scattering peak on a magnified scale. The peak at approximately 0.3 nm^{-1} is the result of imperfect background subtraction of the Kapton windows that were used to contain the sample. Similarly, the baseline intensity observed at high values of q is an artifact of

Table 2. Characteristics of the Electrolytes in This Study

polymer	r [Li$^+$]/[EO]	$\phi_{\mathrm{EO/salt}}$	morphology	T_{ODT} °C
SEO(1.9−0.8)	0.03	0.31	DIS	
	0.05	0.32	DIS	
	0.085	0.34	DIS	
	0.10	0.35	LAM → DIS	107.5
	0.125	0.37	LAM	
	0.15	0.38	LAM	
	0.20	0.41	LAM	
	0.25	0.43	LAM	
SEO(1.4−1.6)	0.03	0.55	DIS	
	0.05	0.56	DIS	
	0.085	0.59	DIS	
	0.10	0.60	DIS	
	0.125	0.61	HEX → DIS	62.5
	0.15	0.63	HEX → DIS	107.5
	0.20	0.65	HEX	
	0.25	0.67	HEX	
SEO(1.7−1.4)	0.01	0.45	DIS	
	0.03	0.47	DIS	
	0.04	0.47	DIS	
	0.065	0.49	LAM → DIS	82.5
	0.075	0.50	LAM → DIS	107.5
	0.085	0.51	LAM → DIS	117.5
	0.10	0.52	LAM	
	0.125	0.53	LAM	
	0.15	0.55	LAM	
	0.17	0.56	LAM	
	0.20	0.57	GYR	
	0.25	0.60	GYR	
SEO(2.9−3.3)	0.005	0.53	DIS	
	0.01	0.53	DIS	
	0.015	0.54	LAM → DIS	62.5
	0.02	0.54	LAM → DIS	107.5
	0.025	0.54	LAM → DIS	132.5
	0.03	0.55	LAM	
	0.04	0.56	LAM	
	0.05	0.56	LAM	
	0.085	0.59	LAM	
	0.10	0.60	LAM	
	0.125	0.61	LAM/GYR	
	0.15	0.63	GYR	
	0.20	0.65	HEX	
SEO(4.9−5.5)	0.0025	0.52	LAM → DIS	102.5
	0.005	0.52	LAM → DIS	137.5
	0.01	0.53	LAM	
	0.03	0.54	LAM	
	0.05	0.56	LAM	
	0.085	0.58	LAM	
	0.10	0.59	LAM	
	0.125	0.61	LAM	
	0.15	0.62	LAM	
	0.20	0.65	LAM	
	0.25	0.67	HEX	
SEO(6.4−7.3)	0.085	0.59	LAM	

dx.doi.org/10.1021/jp408079z | J. Phys. Chem. B 2014, 118, 4−17

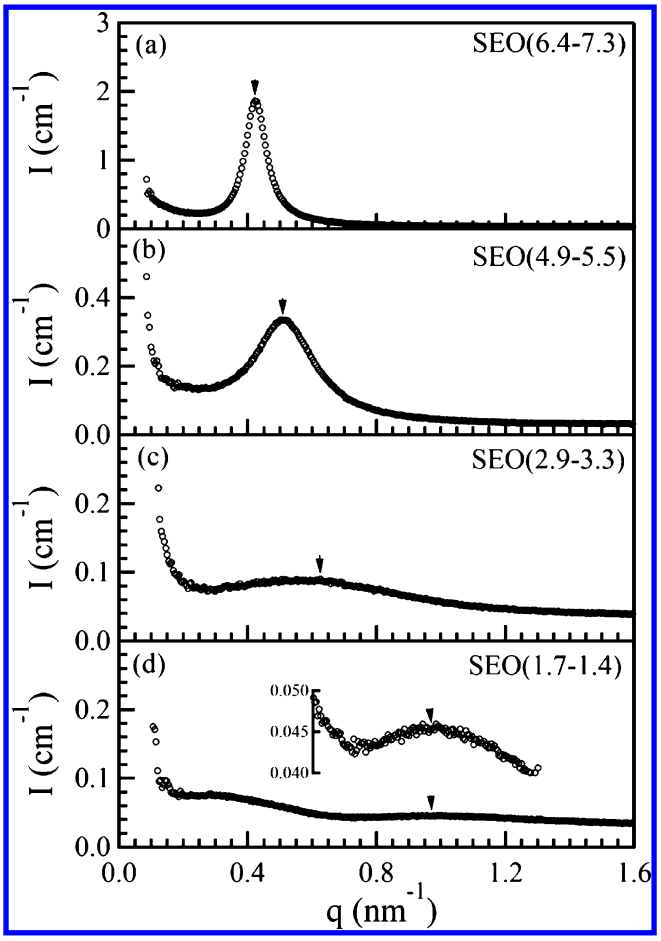

Figure 2. (a–d) SAXS profiles of a series of neat, symmetric SEO copolymers at 110 °C.

imperfect background subtraction of the empty cell. These effects are most pronounced in Figure 2d because of the extremely low scattering observed from this sample.

The scattering theory of monodisperse disordered block copolymers was developed by Leibler.[23] The scattering function $I(q)$ proposed by this theory for a perfectly monodisperse AB diblock copolymer with degree of polymerization N can be written as

$$I_{dis}(q) = \nu_{ref}\left(\frac{b_A}{\nu_A} - \frac{b_B}{\nu_B}\right)^2\left[\frac{S(q)}{W(q)} - 2\chi\right]^{-1} \quad (7)$$

where b_A and b_B are the X-ray scattering lengths of blocks A and B, respectively; ν_A and ν_B are the monomer volumes of A and B, respectively; and ν_{ref} is a reference volume. $W(q)$ and $S(q)$ are the determinant and sum of the elements, respectively, of the structure factor matrix $\|\mathbf{S}_{ij}\|$. In this work, the reference volume is 0.1 nm^3. The expressions $W(q)$ and $S(q)$ are given by

$$W(q) = S_{AA}(q)S_{BB}(q) - S_{AB}^2(q) \quad (8)$$

$$S(q) = S_{AA}(q) + S_{BB}(q) + 2S_{AB}(q) = Ng(1) \quad (9)$$

with

$$S_{AA}(q) = Ng(f) \quad (10)$$

$$S_{BB}(q) = Ng(1-f) \quad (11)$$

$$S_{AB}(q) = (N/2)[g(1) - g(f) - g(1-f)] \quad (12)$$

$$g(f) = (2/x^2)[fx + \exp(-fx) - 1] \quad (13)$$

and

$$x = q^2R_g^2 \quad (14)$$

$$R_g^2 = Na^2/6 \quad (15)$$

where S_{AA}, S_{AB}, and S_{BB} are the pairwise elements of the structure factor matrix, $g(f)$ is the form factor for a Gaussian chain, and R_g is the radius of gyration of the copolymer. The polydispersity of a copolymer has been shown to affect its scattering. In the case of neat copolymers, the volume fraction term f in eqs 10–16 is equal to ϕ_{EO} as defined by eq 1. Since our copolymers are not perfectly monodisperse, the expression $I(q)$ was modified to reflect their nonideality by assuming a Schultz–Zimm distribution for total molecular weight.[7] In this case, eq 13 is replaced by

$$g(f) = (2/x^2)\{fx - 1 + [k/(k+fx)]^k\} \quad (16)$$

where

$$k = 1/(\mathrm{PDI} - 1) \quad (17)$$

and N in eqs 9–12 and 14 is the number-averaged degree of polymerization. More detailed discussion of limitations, assumptions, and justifications for using the particular form of the scattering equations shown above can be found in Mori et al.[7] A k value of 28.5, which corresponds to a PDI of approximately 1.04, was used for all fitting. Our results are not sensitive to the exact value of k used in the calculations over the range of PDIs in Table 1. In the discussion below, all values of N are number-averaged, and all values of χ are obtained by fitting the experimental scattering curves from disordered samples to eq 7.

The only adjustable parameters for fitting the absolute scattering of a neat copolymer to the scattering function $I_{dis}(q)$ in eq 7 are R_g and χ. Figure 3 is, as an example of the fitting

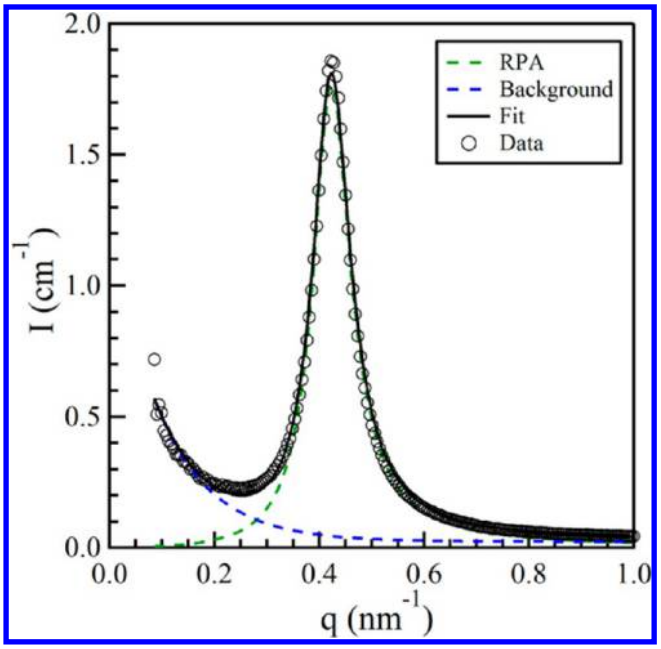

Figure 3. Comparison of the experimental and calculated SAXS profiles for neat SEO(6.4–7.3) at 110 °C. The fit is the sum of the background and the RPA results.

dx.doi.org/10.1021/jp408079z | J. Phys. Chem. B 2014, 118, 4–17

performed in this study, showing the absolute scattering of SEO(6.4−7.3) at 110 °C. The open symbols show the data, and the solid line represents a fit to the equation

$$I(q) = I_{dis}(q) + I_{bgd}(q) \tag{18}$$

where $I_{bgd}(q)$ is an exponential decay to compensate for the imperfect background subtraction that occurs near the beamstop. The fit shows excellent agreement with the data over the entire range. Figure S1 of the Supporting Information shows the sensitivity of the fit to R_g and χ, confirming the accuracy of the values determined by this procedure.

Figure 4 shows the temperature dependence of χ_0 for the neat block copolymers. These values were obtained from the fit

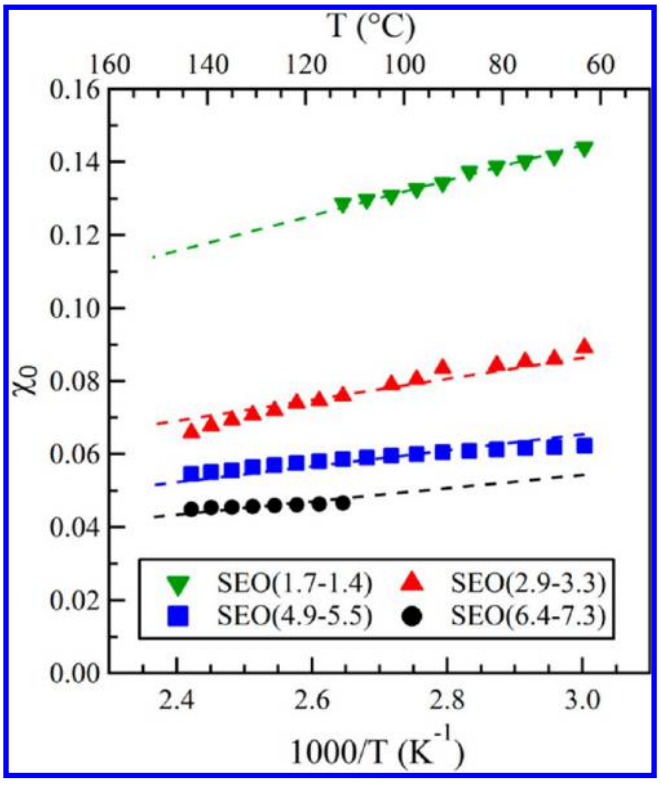

Figure 4. Temperature dependence of χ_0 for a series of neat, symmetric SEO block copolymers. The dashed lines are fits of the data to eq 19.

of eq 7 to the 1D scattering profiles of disordered samples. SEO(6.4−7.3) is ordered at $T < 105$ °C, preventing values of χ_0 from being obtained for those temperatures. The scattering from SEO(1.4−1.6) and SEO(1.9−0.8) at all temperatures as well as that from SEO(1.7−1.4) at $T > 105$ °C is indistinguishable from the background, preventing values of χ_0 from being determined; this is a consequence of the small degree of polymerization of the copolymers and the relatively low scattering contrast between blocks. The dotted lines indicate a fit of the data to

$$\chi_0 = \frac{K}{T} \tag{19}$$

It is clear that χ_0 is not independent of chain length. While this dependence is often ignored, it has been reported in polystyrene-*b*-polyisoprene (PS-*b*-PI) copolymers.[7,8] Figure 5 shows χ_0 as a function of $1/N$ for the neat copolymers at 60 and 140 °C. The dotted lines represent a fit to

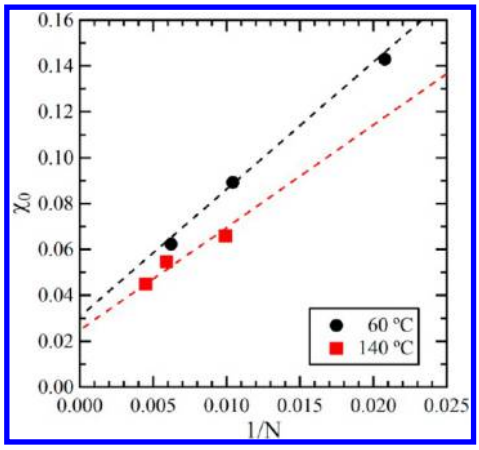

Figure 5. Chain length, N, dependence of χ_0 for a series of neat, symmetric SEO block copolymers at 60 and 140 °C. The dashed lines represent eq 20 using parameters given in the text.

$$\chi_0 = A(T) + \frac{B(T)}{N} \tag{20}$$

where $A(T) = 10.2 \times T^{-1}$ and $B(T) = 1.85 \times 10^3 \times T^{-1}$. This functional form implies that, at infinite N, χ_0 becomes a simple function of $1/T$. It also indicates that, even at $N \approx 10^3$, a 10% difference in χ_0 is expected compared to χ_0 at infinite N. Several other functional forms were tested; however, no other expression resulted in as good a fit to the data.

Ion-Containing Copolymers. Figure 6a shows the SAXS profiles of SEO(2.9−3.3) at 60 °C in the neat state and at selected salt concentrations. In the neat state, the polymer exhibits a single broad low-intensity peak at $q^* = 0.658$ nm^{-1}, corresponding to a domain spacing of 9.6 nm. At $r = 0.01$, the copolymer is still disordered, but the peak has become much more pronounced, and the q^* peak has shifted to lower q. The addition of more salt in the $r = 0.10$ sample results in the appearance of a sharp primary scattering peak with higher-order reflections at $q/q^* = 1$, 2, 3, and 4, indicating the presence of well-ordered LAM. The $r = 0.15$ sample exhibits peaks at $q/q^* = 1$, $\sqrt{(4/3)}$, $\sqrt{(7/3)}$, $\sqrt{(15/3)}$, $\sqrt{(16/3)}$, $\sqrt{(19/3)}$, $\sqrt{(20/3)}$, $\sqrt{(21/3)}$, $\sqrt{(23/3)}$, $\sqrt{(24/3)}$, and $\sqrt{(25/3)}$, indicating the GYR phase, while the $r = 0.20$ sample shows peaks at $q/q^* = \sqrt{4}$, $\sqrt{7}$, $\sqrt{12}$, and $\sqrt{13}$, indicating HEX. Experiments similar to those reported in Figure 6a were repeated at temperatures between 60 and 140 °C. These results are summarized in Figure 6b, which shows the overall phase behavior of SEO(2.9−3.3) as a function of salt concentration. The open circles (○) indicate observed coexistence between adjacent phases, the dashed lines (-) represent boundaries between phases, and the shaded areas represent regions of coexistence. In the neat state and at low salt concentrations, the copolymer is disordered. As salt is added to the copolymer, χ_{eff} and $\phi_{EO/salt}$ begin to increase, and the sample gains a weakly ordered lamellar morphology with accessible order−disorder transitions (ODTs). The ODT temperature T_{ODT} of the electrolyte increases as the salt concentration r increases from 0.015 to 0.025. At salt concentrations from $r = 0.03$ to $r = 0.10$, the copolymer retains the lamellar morphology over the entire temperature range. At $r = 0.125$, we observe coexistence of the lamellar and gyroid phases before observing the pure gyroid phase at $r = 0.15$. At the highest salt concentration tested for this copolymer, $r = 0.20$, HEX are observed at all temperatures. Phase boundaries in Figure 6b were placed at the midpoint

dx.doi.org/10.1021/jp408079z | J. Phys. Chem. B 2014, 118, 4−17

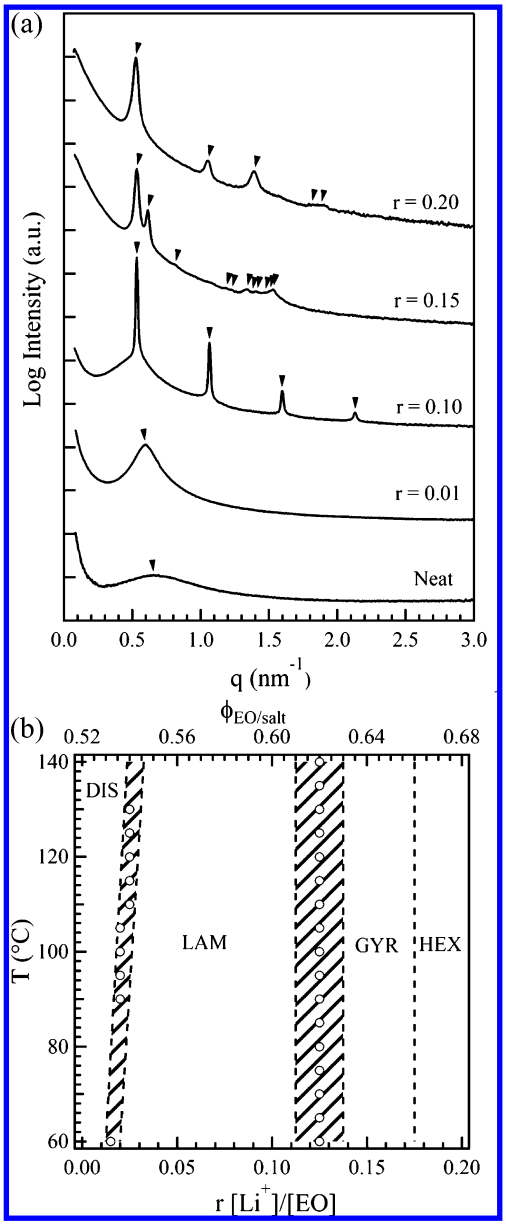

Figure 6. (a) SAXS profiles at 60 °C for SEO(2.9−3.3) at several salt concentrations. Profiles are offset vertically for clarity. The arrows represent the locations of primary and higher order scattering peaks. (b) Phase diagram of SEO(2.9−3.3)/LiTFSI as a function of salt concentration r. Dashed lines mark phase boundaries, and open circles (○) indicate observed coexistence.

between different observed morphologies. For example, the sample with r = 0.15 was GYR, while that with r = 0.20 was HEX.

The effect of salt addition on χ_{eff} between the blocks can be measured directly via RPA fitting of SAXS profiles obtained from disordered electrolytes; however, introducing salt to the copolymer presents two minor complications:

(1) The first complication is that the addition of salt predicates coexistence between phases, as is required by the Gibbs phase rule for binary mixtures. This means that the transition from order to disorder, or the transition between ordered phases, is expected to occur continuously over a region of coexistence. This is observed experimentally by the apparent superposition of scattering profiles from the two phases. This is illustrated in Figure 7, which shows the absolute intensity scattering profile of SEO(2.9−3.3) with r = 0.02 at 105 °C. The

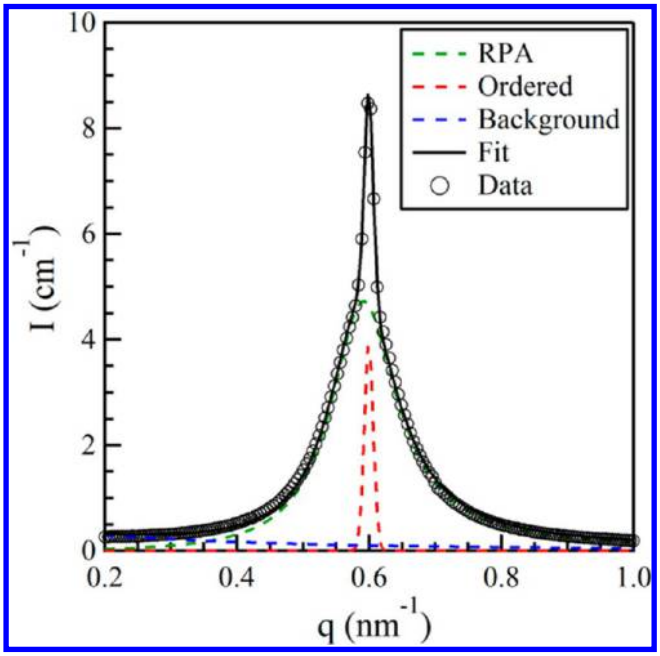

Figure 7. Comparison of the experimental and calculated SAXS profiles for neat SEO(2.9−3.3), r = 0.02 at 105 °C. Coexistence between the ordered and disordered state is observed. The calculated fit is the sum of the background, the theoretical RPA calculations, and the ordered peak.

open symbols show the experimental data, and the solid black line shows the fit to

$$I(q) = I_{dis}(q) + I_{ord}(q) + I_{bgd}(q) \tag{21}$$

where $I_{ord}(q)$ is an additional term to account for the scattering from the ordered phase:

$$I_{ord}(q) = K \exp\left(\frac{-(q - q_0)^2}{\sigma^2}\right) \tag{22}$$

where K, σ, and q_0 are fitting parameters. The contribution from the exponential background decreases substantially once salt is introduced to the copolymer, as a result of the larger scattering contrast between phases and the concomitant higher scattering intensity.

(2) The second minor complication is that, since the PEO phase is no longer pure, its scattering length density $B_{EO/salt}$ must be adjusted accordingly. Assuming ideal mixing (no volume change of mixing) and perfect localization of salt in the PEO phase, the new scattering length density of the PEO/LiTFSI phase can be calculated by

$$B^{ideal}_{EO/salt} = Y_{LiTFSI}B_{LiTFSI} + (1 - Y_{LiTFSI})B_{EO} \tag{23}$$

where

$$B_i = \frac{b_i}{v_i} \tag{24}$$

and Y_{LiTFSI} is the volume fraction of LiTFSI in the PEO/LiTFSI microphase calculated by

dx.doi.org/10.1021/jp408079z | J. Phys. Chem. B 2014, 118, 4−17

$$Y_{salt}(r) = \frac{r\rho_{EO}M_{LiTFSI}}{r\rho_{LiTFSI}M_{EO} + r\rho_{EO}M_{LiTFSI}} \quad (25)$$

It is well known that salt solutions do not obey the ideal mixing rule. For this reason, we left $B_{EO/salt}$ as an additional fit parameter to achieve the best fit to the data. The scattering length density obtained from this fit is called $B^{fit}_{EO/salt}$. Thus, for a fully disordered salt-containing copolymer, the number of fit parameters was increased by one relative to the pure copolymer.

We can calculate the density of the PEO/LiTFSI microphase $\rho^{fit}_{EO/salt}$ using

$$\rho^{fit}_{EO/salt} = B^{fit}_{EO/salt}(\rho^{ideal}_{EO/salt}/B^{ideal}_{EO/salt}) \quad (26)$$

where

$$\rho^{ideal}_{EO/salt} = \frac{1 + (rM_{LiTFSI}/M_{EO})}{(1/\rho_{EO}) + (rM_{LiTFSI})/(\rho_{LiTFSI}M_{EO})} \quad (27)$$

Figure 8a shows the values for $\rho^{fit}_{EO/salt}$ of all the disordered samples at 140 °C. The dashed black line represents the ideal density of the PEO/salt microphase that was calculated on the basis of eq 27. Deviations from ideal mixing are shown clearly in Figure 8b, which presents the ratio of $\rho^{fit}_{EO/salt}$ to $\rho^{ideal}_{EO/salt}$ for all disordered samples as a function of r. At low salt concentration, the fitted density is greater than expected, and at high salt concentration, the fitted density is lower than expected, with a crossover salt concentration of about $r = 0.085$. It is interesting to note that the crossover value of $r = 0.085$ coincides with the salt concentration at which maximum conductivity is observed in this system.[3] The values of $\rho^{fit}_{EO/salt}$ never varied by more than ±5% of the ideal value. These seemingly insignificant deviations in $\rho_{EO/salt}$ are important during the calculation of the scattering contrast because the electron density of the two phases of interest are similar: while a 5% increase in $\rho_{EO/salt}$ results in a 100% increase in $(B_{EO/salt} - B_{PS})^2$, a 5% decrease of the former results in a 27% decrease of the latter.

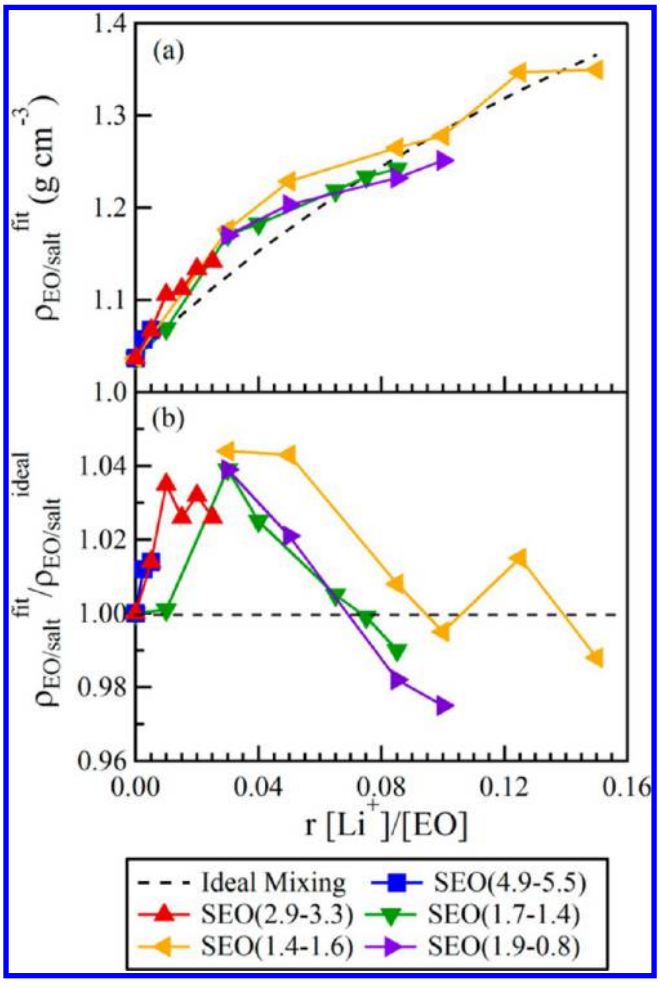

Figure 8. (a) Fitted density of PEO/salt microphase $\rho^{fit}_{EO/salt}$. (b) Ratio of fitted to ideal density of PEO/salt microphase $\rho^{fit}_{EO/salt}/\rho^{ideal}_{EO/salt}$ versus salt concentration r for all disordered electrolytes at 140 °C. The dashed lines represent the density of ideal mixtures.

The fitting procedure described above was used to measure the effect of r on χ_{eff} for each of the polymers in this study. In the case of salt-containing copolymers, the volume fraction term f in eqs 10-16 is equal to $\phi_{EO/salt}$ as defined by eq 5. The salt concentration for each polymer was increased in small increments from zero to the concentration at which an ODT was no longer accessible in the experimental temperature window. The salt concentration at which this occurred depended on the values of N and ϕ_{EO} of the polymer. Figure 9 shows plots of χ_{eff} versus inverse temperature for the series of symmetric copolymers over the full range of salt concentration. The volume fraction $\phi_{EO/salt}$ of all samples shown here are between 0.44 and 0.54. The full symbols indicate the sample was fully disordered, while the open symbols denote that coexistence was observed at this temperature, such as in Figure 7. Figure 9a shows the χ_{eff} values for SEO(4.9−5.5) at $r = 0$, 0.0025, and 0.005. The pure copolymer has a relatively high χN value and needs only a small quantity of salt to induce ordering; it exhibits an ODT at very small concentrations and becomes permanently ordered at $r = 0.01$. Figure 9b shows the χ_{eff} values for SEO(2.9−3.3) at $r = 0$, 0.005, 0.01, 0.015, 0.02, and 0.025. There is a large increase in χ_{eff} between $r = 0$ and $r = 0.005$, especially at higher temperatures. As the value of r increases, the subsequent increases in χ_{eff} decrease in magnitude. Figure 9c shows the χ_{eff} values for SEO(1.7−1.4) at $r = 0$, 0.01, 0.03, 0.04, 0.065, 0.075, and 0.085. Once again we observed a large increase in χ_{eff} values at low salt concentrations and smaller increases in χ_{eff} as the value of r increased. At the highest salt concentrations, χ_{eff} is nearly independent of r.

We show the values of χ_{eff} obtained from different symmetric copolymers as a function of salt concentration at 60 and 140 °C in Figure 10a,b, respectively. There are several things worth noting in these plots: (1) The lack of collapse of the data in these plots indicates that χ_{eff} is a strong function of chain length N as first described in Figures 4 and 5 in the context of χ_0 for salt-free samples. (2) The relationship between χ_{eff} and r is highly nonlinear, with a sharp initial increase at low salt concentration, followed by an apparent saturation. (3) The magnitude of the increase in χ_{eff} with r depends strongly on the chain length of the copolymer. This complex behavior can be captured by an extension of eq 20 to

$$\chi_{eff} = A(T) + \frac{B(T)}{N} + \frac{C(T)}{N}\left[1 - \exp\left(\frac{-D(T)r}{N}\right)\right] \quad (28)$$

where $C(T) = 1.01 \times 10^{-2} \times T$ and $D(T) = 22.4 \times T$. The dotted lines in Figure 10 are the results obtained by plotting eq 28 with N values given by eq 3. This remarkably simple expression, with four adjustable parameters, accurately captures

dx.doi.org/10.1021/jp408079z | J. Phys. Chem. B 2014, 118, 4−17

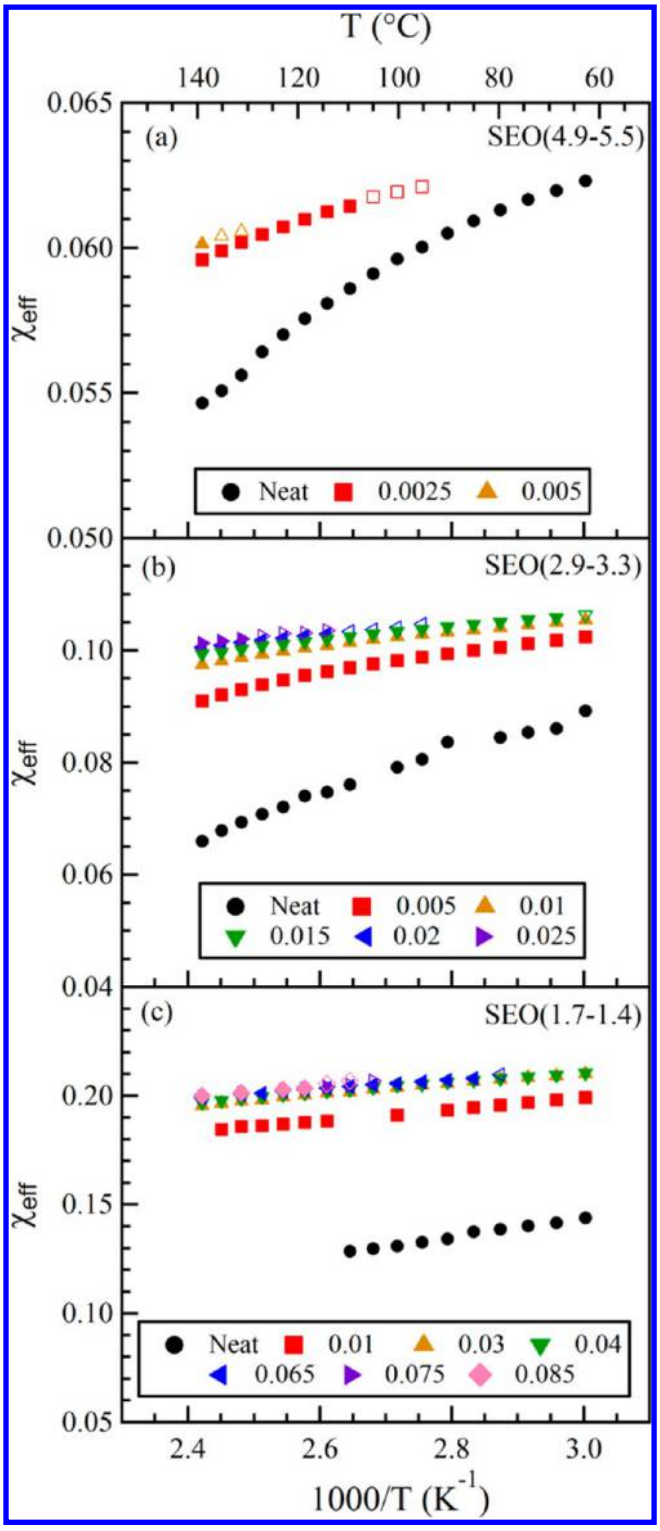

Figure 9. Effective interaction parameter χ_{eff} versus inverse temperature for (a) SEO(4.9−5.5), (b) SEO(2.9−3.3), and (c) SEO(1.7−1.4) at a series of salt concentrations. The full symbols indicate the sample was fully disordered, while the open symbols denote that coexistence was observed at this temperature.

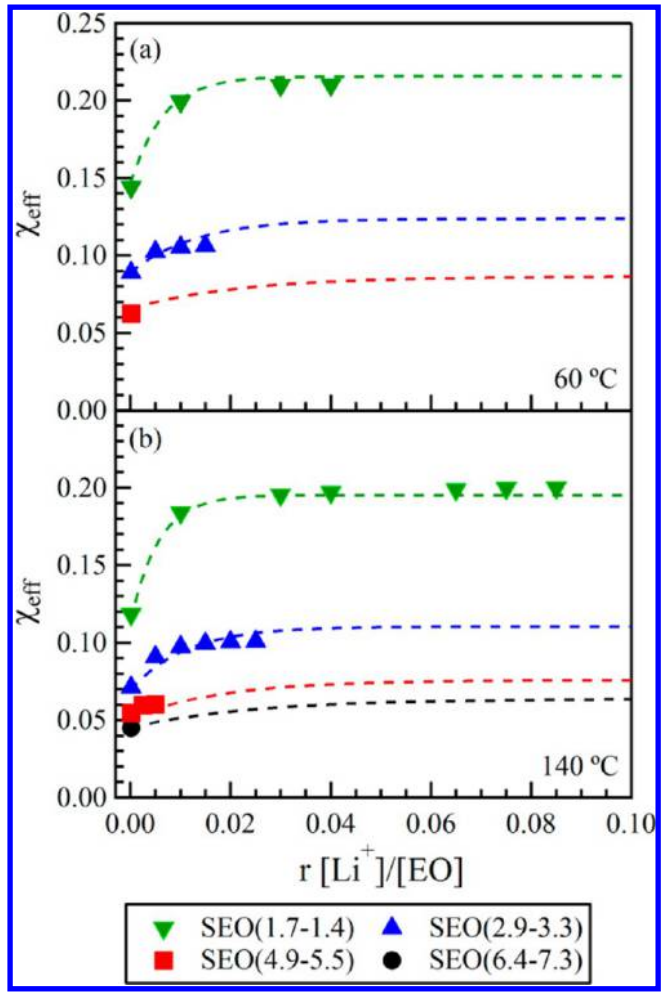

Figure 10. Effective interaction parameter χ_{eff} versus salt concentration r for a series of symmetric diblock SEO copolymers at (a) 60 and (b) 140 °C. The dashed lines represent eq 28 using parameters given in the text.

the behavior seen by all the symmetric copolymers at all temperatures and salt concentrations. Several other functional forms were tested; however, no other expression resulted in as good a fit to the data. It is important to note that, because our approach for measuring χ requires disordered samples, the window over which χ can be measured in our approach closes rapidly with increasing molecular weight. The extent to which eq 28 applies to molecular weights that are not covered explicitly in our study remains to be established. Nevertheless, eq 28 implies that, in the high molecular weight limit, the addition of salt to the copolymer is expected to have a negligible effect on χ_{eff}.

Two additional polymers examined in this study were asymmetric. Figure 11a shows χ_{eff} versus inverse temperature for SEO(1.4−1.6) at a range of salt concentrations, where $\phi_{EO/salt}$ ranges from 0.55 to 0.63. The full symbols indicate the sample was fully disordered, while the open symbols denote that coexistence was observed at that temperature. The value of χ_{eff} increases with increasing salt concentration, with small variations in slope. Figure 11b shows χ_{eff} versus inverse temperature for SEO(1.9−0.8) at a range of salt concentrations, where $\phi_{EO/salt}$ ranges from 0.31 to 0.35. The most noteworthy feature of this plot is that χ_{eff} decreases as the salt concentration is increased. To our knowledge, these are the first experimental data showing that the addition of salt can induce mixing in diblock copolymers.

Figure 12 shows χ_{eff} as a function of r for the asymmetric SEO copolymers. The values of χ_{eff} for SEO(1.4−1.6) increase steadily as a function of r, while they decrease for SEO(1.9−

dx.doi.org/10.1021/jp408079z | J. Phys. Chem. B 2014, 118, 4−17

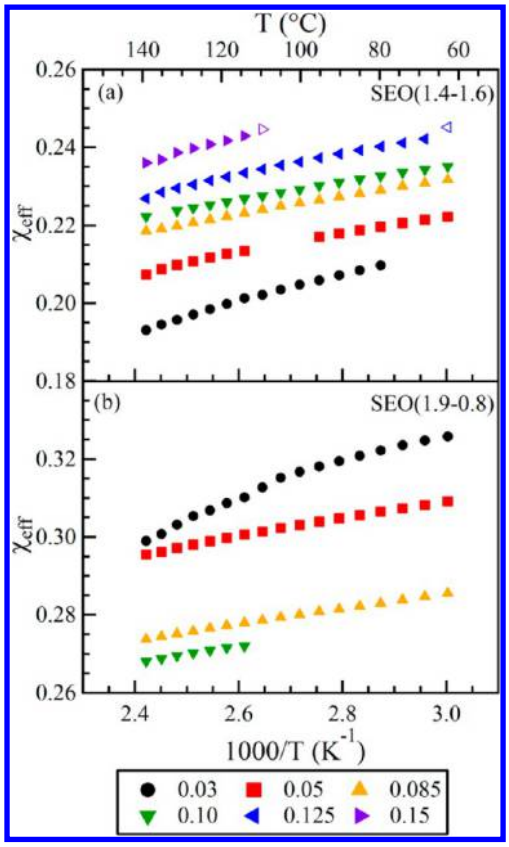

Figure 11. Effective interaction parameter χ_{eff} versus inverse temperature for (a) SEO(1.4−1.6) and (b) SEO(1.9−0.8) at a series of salt concentrations. The full symbols indicate the sample was fully disordered, while the open symbols denote that coexistence was observed at this temperature.

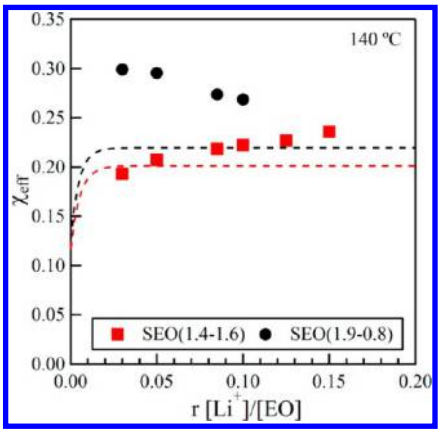

Figure 12. Effective interaction parameter χ_{eff} versus salt concentration r for SEO(1.4−1.6) and SEO(1.9−0.8) at 140 °C. The dashed lines represent eq 28 using parameters given in the text. The red and black dashed line correspond to SEO(1.4−1.6) and SEO(1.9−0.8), respectively.

0.8). The dotted lines are the results obtained by plotting eq 28 with N values given by eq 3. Not surprisingly, the data from SEO(1.9−0.8) are qualitatively different from predictions based on eq 28. We offer no explanation for the departure of the data in Figure 12 from the values predicted by eq 28.

The data collected in this study are summarized in Figure 13 by plotting all the disordered samples onto a diagram that resembles a conventional block copolymer phase diagram. The abscissa in Figure 13 is the volume fraction of the ion-containing phase $\phi_{EO/salt}$, and the ordinate is $\chi_{eff}(N,r)N$. The data for each sample, represented by three open symbols to indicate T = 60, 100, and 140 °C, are connected by a line. The values for $\phi_{EO/salt}$ are calculated by eq 5, and the values for χ_{eff} are determined using eq 18. Worth noting is that, because of the choice of a fixed v_{ref}, as T increases from 60 to 140 °C, N increases, while χ decreases. Depending on the magnitude of the change in χ with T, the value of χN of a given sample may change very little in Figure 13 or in some cases even increase as T increases. The filled symbols show χN at the ODT for all the neat and salty copolymer samples. These data points appear to reconstruct the expected parabolic shape of the diblock copolymer phase envelope, confirming the veracity of our approach. Numerous such plots of phase envelopes exist in the literature.[24,25] In all cases, observations of phase behavior are used to determine χ. Figure 13 is unique not only because χ is determined independently from disordered state scattering profiles but also because χ is an explicit function of N.

The multitude of morphology data collected in this study are summarized in Figure 14 by recasting the results onto a diagram that resembles a conventional block copolymer phase diagram, using the same axes as in Figure 13. The data for each of the samples listed in Tables 1 and 2, represented by three symbols to indicate T = 60, 100, and 140 °C, are connected by a line. The values for $\phi_{EO/salt}$ are calculated by eq 5, and the values for χ_{eff} are calculated using eq 28. Circles (●) represent the disordered state, square symbols (■) represent a lamellar morphology, a cross (×) denotes the gyroid morphology, and the triangles (▲) denote HEX. Open symbols (○) and (□) signify that coexistence was observed at that temperature. Phase boundaries, represented by dashed lines (-), are meant to guide the eye. Samples of SEO(1.4−1.6) and SEO(1.9−0.8) have been omitted due to their lack of conformity to eq 28. This diagram marries the experimentally observed phase behavior with the expected $\chi_{eff}(N,r)N$ and $\phi_{EO/salt}$ values obtained from the fitting equations.

In addition to measuring χ, the fitting of the scattering data also yields values of R_g for each sample. The domain spacing for the disordered sample can be determined by

$$d = DR_g \tag{29}$$

where D is the periodicity of the copolymer and is a function of ϕ. For monodisperse samples, the dependence of D on ϕ is given in ref 23. More detail regarding the approach we used to determine D as well as comparisons of values of D obtained from our procedure with those obtained from ref 23 can be found in the Supporting Information. The domain spacing for the ordered samples can be determined by $d = 2\pi/q_0$. Figure 15 is a comprehensive set of data showing the temperature dependence of the domain spacing for each of the polymers and salt concentrations with an accessible ODT measured in this study. The full symbols indicate the disordered domain spacing, while the open symbols denote the ordered domain spacing. At temperatures for which two domain spacings are reported for a single sample, coexistence was observed. In almost all circumstances, the domain spacing increased monotonically as a function of salt concentration and decreased as a function of temperature.

Figure 16 shows the normalized domain spacing $d/R_{g,0}$ for all the copolymers and salt concentrations in this study at 80 °C, including those without an accessible disordered state, where $R_{g,0}$ is the calculated radius of gyration of the neat diblock. An

dx.doi.org/10.1021/jp408079z | J. Phys. Chem. B 2014, 118, 4−17

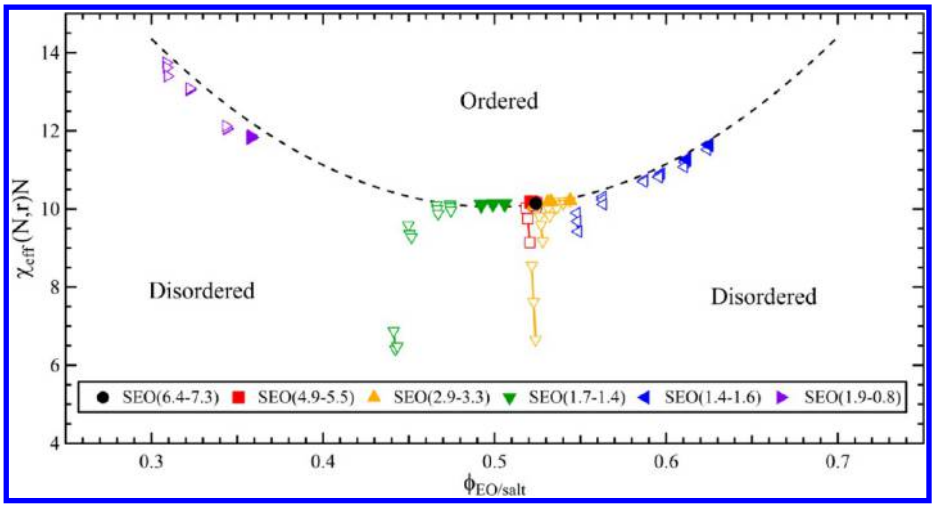

Figure 13. Values of $\chi_{eff}N$ versus $\phi_{EO/salt}$ for all disordered samples in this study. The data for each sample, represented by three open symbols to indicate T = 60, 100, and 140 °C, are connected by a line. The filled symbols show $\chi_{eff}N$ at T_{ODT} for each ODT observed. The dashed line is merely a guide for the eye.

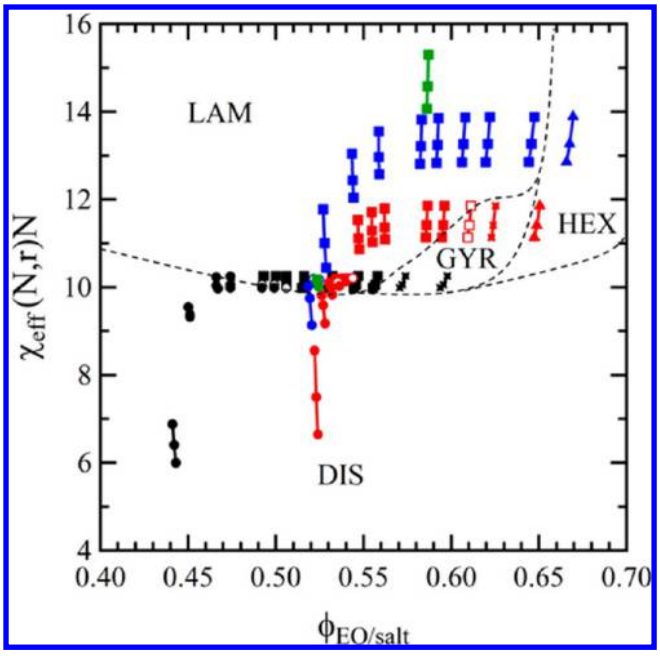

Figure 14. SEO/salt phase diagram calculated from eqs 5 and 28. The data for each sample, represented by three symbols to indicate T = 60, 100, and 140 °C, are connected by a line. (●) represents DIS; (■) represents LAM; (×) denotes GYR; and (▲) denotes HEX. Open symbols (○) and (□) signify that coexistence was observed. Phase boundaries, represented by dashed lines (-), are meant to guide the eye.

analogous plot featuring the absolute values of d for each of the electrolytes is shown in Figure S2 of the Supporting Information. Clearly, the normalized domain spacing is a nonlinear function of r, increasing steeply when r increases from 0 to 0.05, followed by a more gradual increase when r increases from 0.05 to 0.25. The functional form of $d/R_{g,0}$ versus r in Figure 16 is similar to that of χ_{eff} versus r in Figure 10. However, $d/R_{g,0}$ increases from about 3.7 to 5.7 for SEO(4.9−5.5) when r increases from 0 to 0.25 and only increases from 3.7 to 4.6 for SEO(1.7−1.4) over the same range of r. Thus the polymers with longer chain length show the largest increase in normalized domain spacing with salt loading. This is in contrast to the trends seen with χ_{eff} in Figure 10; polymers with the shortest chain length show the largest increase in χ_{eff} with salt loading.

Empirically we found that the dependence of domain spacing on salt concentration obtained for most samples collapsed when $d\chi_{eff}^{2/3}$ was plotted versus r as shown in Figure 17. The collapse was observed for all samples with the exception of the SEO(1.9−0.8), the polymer with the lowest value of ϕ_{EO}. The data in Figure 17 suggest that the product of $d \times \chi_{eff}^{2/3}$ at a given salt concentration is constant, which in turn suggests that d and χ_{eff} are inversely related to each other. It is evident from Figures 16 and 17 that the relationship between χ_{eff} and d is not simple and that traditional relationships between d and χ cannot be used. Figure S3 of the Supporting Information shows explicitly that the oft-cited $N^{2/3}\chi^{1/6}$ versus d relationship does not hold for salt-containing samples; it is thus not possible to estimate values of χ_{eff} from measurements of d.

Comparison with Previous Work. Significant experimental and theoretical effort has been undertaken to understand and quantify the effect of salt addition on χ_{eff}. Wang et al.[26] used small-angle neutron scattering (SANS) to directly measure χ_{eff} on a polystyrene-*b*-poly(methyl methacrylate) (PS-*b*-PMMA) copolymer that was complexed with lithium chloride, while Naidu et al.[11] used SAXS to measure χ_{eff} on a polystyrene-*b*-poly(2-vinyl pyridine) (PS-*b*-P2VP) copolymer that was doped with lithium perchlorate. Young et al.[10] and Huang et al.[9] used domain spacing as a proxy to study χ_{eff} in both an SEO copolymer that was mixed with several lithium salts and a poly(ε-caprolactone)-*b*-poly(ethylene oxide) (PCL-*b*-PEO) that was complexed with lithium perchlorate. The effect of salt on χ_{eff} was determined from order−disorder transition (ODT) measurements by Wanakule et al.[13] using a series of SEO copolymers complexed with LiTFSI and by Gunkel et al.[12] using both an SEO copolymer and a PS-*b*-P2VP copolymer complexed with lithium triflate. Nakamura et al.[14,15] and Wang et al.[16] have published a series of theoretical papers studying the problem using self-consistent field theory and the Born energy of solvation.

The results presented in Figure 10 appear contrary to almost every other study, both experimental and theoretical, that has attempted to determine the relationship between χ_{eff} and r. All previous studies assume that χ_{eff} was a linear function of r, that

dx.doi.org/10.1021/jp408079z | J. Phys. Chem. B 2014, 118, 4−17

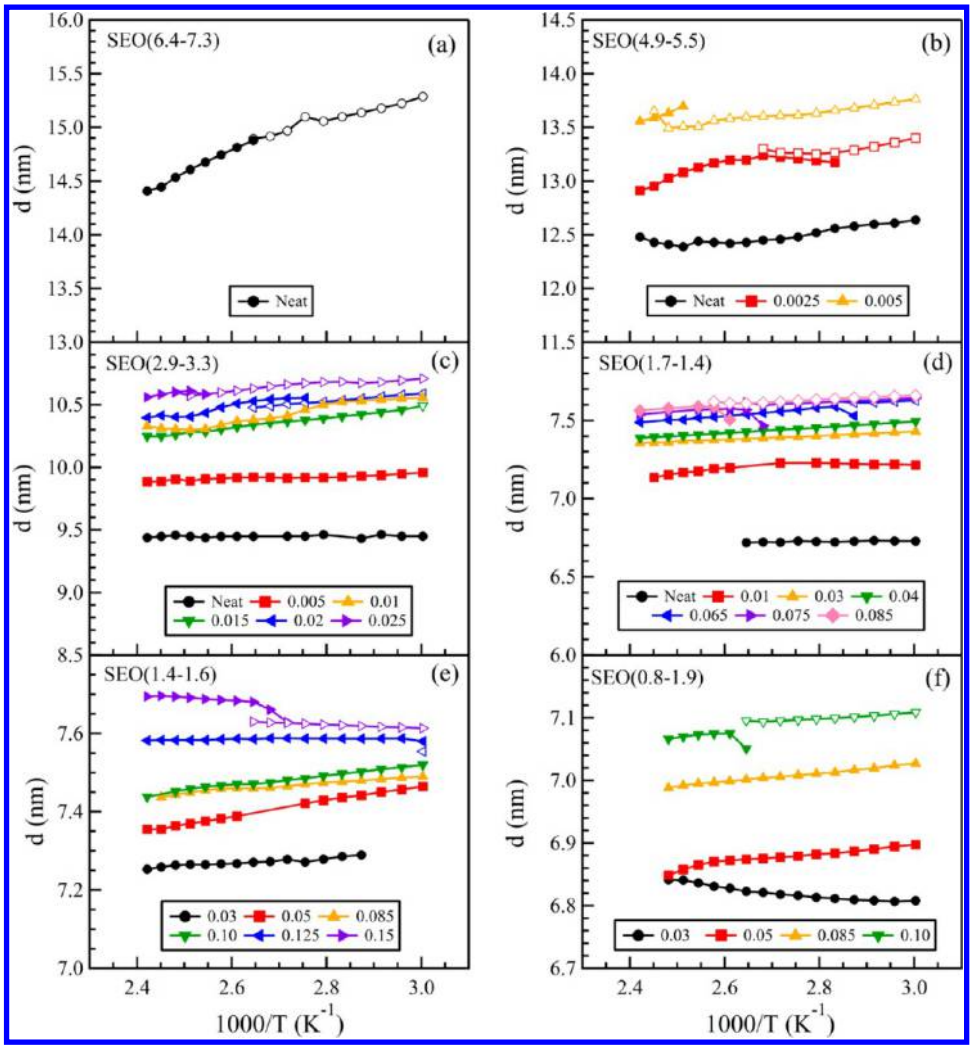

Figure 15. Domain spacing d versus inverse temperature for (a) SEO(6.4−7.3), (b) SEO(4.9−5.5), (c) SEO(2.9−3.3), and (d) SEO(1.7−1.4) at a series of salt concentrations. Solid and open data points indicate disordered and ordered domain spacings, respectively. A coexistence of phases was observed at temperatures for which there exists both a disordered and an ordered domain spacing for a given salt concentration.

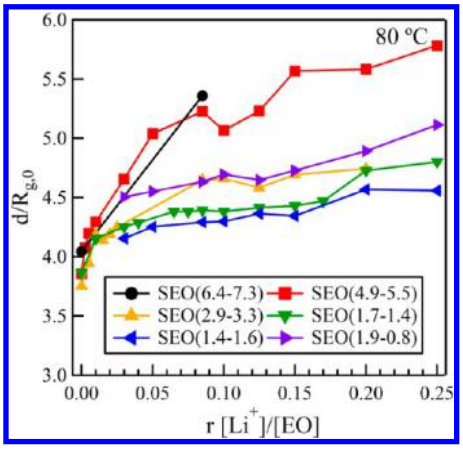

Figure 16. Normalized domain spacing $d/R_{g,0}$ versus salt concentration r for all samples in this study at 80 °C.

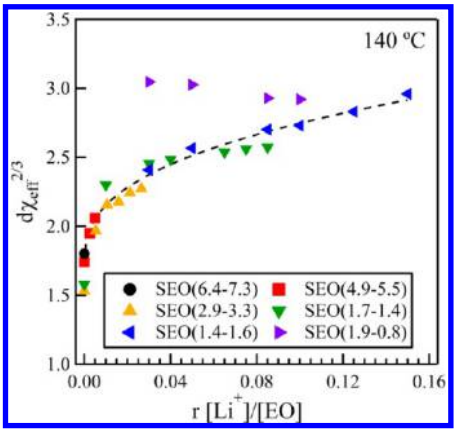

Figure 17. $d\chi_{eff}^{2/3}$ versus salt concentration r for electrolyte at 140 °C. The dashed line is a guide for the eye.

is, $\chi_{eff} = \chi_0 + mr$. Indeed, if one conducts measurements on one polymer and a few salt concentrations, it is easy to see how the relationship may appear linear. The work in refs 9, 11, and 26 is limited to a single block copolymer and a few salt concentrations. Our work clearly shows that the assumptions that were the basis of the analysis in refs 10 and 12 are not valid. In previous work from this lab (ref 13), we ignored the N dependence on χ_0. Surprisingly, the only experimental study to show any indication of the nonlinearity of the relationship contains no comment on the novelty of this observation.[11] The theoretical work by Nakamura et al.[14] suggests that such

dx.doi.org/10.1021/jp408079z | J. Phys. Chem. B 2014, 118, 4−17

nonlinear behavior might be expected if ion clustering of the salt species was occurring in the copolymer. The lack of ion clustering in dilute homopolymer PEO/LiTFSI mixtures ($r < 0.10$) is well established,[27] and the ionic conductivity of high molecular weight SEO/LiTFSI mixtures also does not show evidence of ion clustering.[2,3] However, ion transport in low molecular weight SEO copolymers is considerably more complex, and the data do not rule out the possibility of ion pairing in these systems.[20]

CONCLUSION

Understanding the effect of salt addition on the thermodynamics of block copolymers remains an active area of research, with implications for both fundamental understanding of salt/polymer miscibility as well as for applications such as solid-state electrolytes. However, before this is done, it is important to quantify thermodynamic interactions in neat diblock copolymers. Our results reaffirm that the Flory–Huggins interaction parameter in neat SEO copolymers χ_0 is a strong function of N (Figure 5). Conventional wisdom suggests that the intrinsic Flory–Huggins parameter should be independent of N. Several theoretical papers have attempted to explain the origin of the difference between the χ measured from scattering experiments and the intrinsic Flory–Huggins parameter.[1,28−42] For example, the "intrinsic" Flory–Huggins parameter between PS and PEO in neat block copolymers might be given by $A(T) = 10.2 \times T^{-1}$ (see eq 20), that is, χ_0 in the limit of N tending to infinity. Ignoring the N dependence on χ_{eff} has a profound effect on the interpretation of thermodynamic data from salty samples.

Our experiments on salt-containing block copolymers reveal that the relationship between χ_{eff} and r is highly nonlinear, with a sharp initial increase at low salt concentration followed by an apparent saturation (Figure 10), and that the magnitude of the increase in χ_{eff} with r depends strongly on the chain length of the copolymer. We present a relatively simple expression that captures the behavior of χ_{eff} as a function of salt concentration and chain length for symmetric electrolytes; however, the behavior of asymmetric electrolytes remains poorly understood. In the case of a copolymer with PEO as the minor component, the addition of salt promotes mixing, in contrast to all other reports in the literature, which indicates that the addition of salt promotes demixing. These findings reveal a much more complex relationship between χ_{eff} and salt concentration in block copolymers and represent a significant departure from previous results that asserted a simple linear relationship. Additionally, we demonstrate that changes in domain spacing do not correlate in the expected manner with changes in χ_{eff} for salty copolymer samples.

The results presented in this study are a significant step forward in understanding the effect of salt on block copolymer thermodynamics; yet many questions remain to be answered. Additional experimental and theoretical work is needed to better understand the origin of the data presented in this article.

ASSOCIATED CONTENT

Supporting Information

Further detail about the RPA fitting to the SAXS profiles and about the calculation of domain spacing from the fitted radius of gyration. Additionally, the domain spacing as a function of salt concentration is presented for each of the polymers in this study as well as additional analysis of domain spacing versus interaction parameter. This information is available free of charge via the Internet at http://pubs.acs.org.

AUTHOR INFORMATION

Corresponding Author

*E-mail: nbalsara@berkeley.edu.

Notes

The authors declare no competing financial interest.

Biographies

Alexander Teran received his B.S. in chemical engineering and chemistry from Johns Hopkins University in 2008. He is currently a Ph.D. candidate in chemical engineering at the University of California, Berkeley, where he studies ion transport and thermodynamics of salt-containing block copolymer for use as electrolytes in solid-state lithium metal batteries under the supervision of Nitash Balsara. Photo credit: Lawrence Berkeley National Laboratory—Roy Kaltschmidt, photographer.

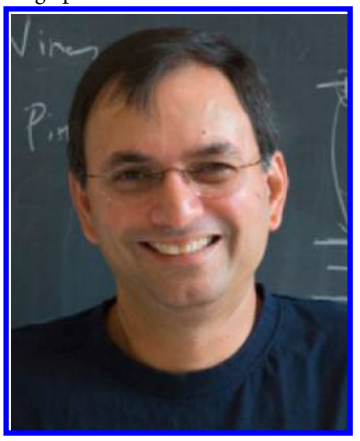

Nitash Balsara is a Professor in the Department of Chemical Engineering at University of California, Berkeley, and a Faculty Senior Scientist at the Lawrence Berkeley National Laboratory. He received a B.S. from the Indian Institute of Technology in Kanpur, India, in 1982, an M.S. from Clarkson University in 1984, and a Ph.D. in Chemical Engineering from Rensselaer Polytechnic Institute in 1988. He did postdoctoral research at the University of Minnesota and at Exxon Research and Engineering Company. His research is concerned with the synthesis and characterization of microstructured polymer materials. Current applications include polymer electrolytes for lithium batteries and membranes for biofuel purification.

ACKNOWLEDGMENTS

The authors thank Dr. Frances Allen and Dr. Andrew Minor for providing the TEM micrograph of the SEO/salt mixture. The synthesis and characterization of the polymer was supported by the Assistant Secretary for Energy Efficiency and Renewable Energy, Office of Vehicle Technologies of the U.S. Department

of Energy under contract DE-AC02-05CH11231 under the Batteries for Advanced Transportation Technologies (BATT) Program. A.A.T. was supported by a National Science Foundation Graduate Research Fellowship. SAXS experiments were performed at the Advanced Light Source, a user facilities at Lawrence Berkeley National Laboratory supported by the Director, Office of Science, Office of Basic Energy Sciences, of the U.S. Department of Energy under Contract DE-AC02-05CH11231.

LIST OF SYMBOLS

a	statistical segment length (nm)
b_i	scattering length of species i (nm mer^{-1})
B_i	scattering length density of species i (nm^{-2} mer^{-1})
d	domain spacing (nm)
D	periodicity
f	volume fraction
I	scattering intensity (cm^{-1})
I_{dis}	disordered copolymer scattering intensity (cm^{-1})
I_{bgd}	background scattering intensity (cm^{-1})
I_{ord}	ordered copolymer scattering intensity (cm^{-1})
M_{PEO}	number-averaged molecular weight of the poly(ethylene oxide) block
M_{PS}	number-averaged molecular weight of the polystyrene oxide block
M_i	number-averaged molecular weight of species i (g mol^{-1})
N	number-averaged degree of polymerization (sites chain^{-1})
N_{avg}	Avogadro's number
N_i	number-averaged degree of polymerization of species i (sites chain^{-1})
q	scattering vector (nm^{-1})
q^*	scattering vector at the primary scattering peak (nm^{-1})
q_0	scattering vector at the ordered scattering peak (nm^{-1})
r	salt concentration ([Li$^+$] [EO]$^{-1}$)
R_g	radius of gyration (nm)
$R_{g,0}$	radius of gyration of neat copolymer (nm)
T	temperature (K)
T_{ODT}	order−disorder transition temperature (K)
Y	volume fraction salt in PEO/LiTFSI microphase (LiTFSI cm^3 PEO/LiTFSI cm^{-3})

Greek

ν_i	molar volume of species i (cm^3 mol^{-1})
ν_{ref}	reference volume (nm^3 site^{-1})
ρ_i	density of species i (g cm^{-3})
ϕ_{EO}	volume fraction of PEO microphase
$\phi_{EO/salt}$	volume fraction of PEO/LiTFSI microphase
χ	interaction parameter
χ_{eff}	interaction parameter of salty SEO copolymer
χ_0	interaction parameter of neat SEO copolymer

REFERENCES

(1) Fredrickson, G. H.; Helfand, E. Fluctuation Effects in the Theory of Microphase Separation in Block Copolymers. *J. Chem. Phys.* **1987**, *87* (1), 697−705.

(2) Singh, M.; Odusanya, O.; Wilmes, G. M.; Eitouni, H. B.; Gomez, E. D.; Patel, A. J.; Chen, V. L.; Park, M. J.; Fragouli, P.; Iatrou, H.; Hadjichristidis, N.; Cookson, D.; Balsara, N. P. Effect of Molecular Weight on the Mechanical and Electrical Properties of Block Copolymer Electrolytes. *Macromolecules* **2007**, *40* (13), 4578−4585.

(3) Panday, A.; Mullin, S.; Gomez, E. D.; Wanakule, N.; Chen, V. L.; Hexemer, A.; Pople, J.; Balsara, N. P. Effect of Molecular Weight and Salt Concentration on Conductivity of Block Copolymer Electrolytes. *Macromolecules* **2009**, *42* (13), 4632−4637.

(4) Fenton, D. E.; Parker, J. M.; Wright, P. V. Complexes of Alkali-Metal Ions with Poly(Ethylene Oxide). *Polymer* **1973**, *14* (11), 589−589.

(5) Armand, M., *Fast Ion Transport in Solids*; North-Holland: Amsterdam, 1973; pp 665−673.

(6) Gray, F. M., *Solid Polymer Electrolytes. Fundamentals and Technological Applications*; VCH: Weinheim, Germany, 1991.

(7) Mori, K.; Okawara, A.; Hashimoto, T. Order−Disorder Transition of Polystyrene-Block-Polyisoprene 0.1. Thermal Concentration Fluctuations in Single-Phase Melts and Solutions and Determination of chi as a Function of Molecular Weight and Composition. *J. Chem. Phys.* **1996**, *104* (19), 7765−7777.

(8) Lin, C. C.; Jonnalagadda, S. V.; Kesani, P. K.; Dai, H. J.; Balsara, N. P. Effect of Molecular Structure on the Thermodynamics of Block-Copolymer Melts. *Macromolecules* **1994**, *27* (26), 7769−7780.

(9) Huang, J.; Tong, Z.-Z.; Zhou, B.; Xu, J.-T.; Fan, Z.-Q. Salt-Induced Microphase Separation in Poly(ϵ-caprolactone)-*b*-poly-(ethylene oxide) Block Copolymer. *Polymer* **2013**, *54* (12), 3098−3106.

(10) Young, W. S.; Epps, T. H. Salt Doping in PEO-Containing Block Copolymers: Counterion and Concentration Effects. *Macromolecules* **2009**, *42* (7), 2672−2678.

(11) Naidu, S.; Ahn, H.; Gong, J.; Kim, B.; Ryu, D. Y. Phase Behavior and Ionic Conductivity of Lithium Perchlorate-Doped Polystyrene-*b*-poly(2-vinylpyridine) Copolymer. *Macromolecules* **2011**, *44* (15), 6085−6093.

(12) Gunkel, I.; Thurn-Albrecht, T. Thermodynamic and Structural Changes in Ion-Containing Symmetric Diblock Copolymers: A Small-Angle X-ray Scattering Study. *Macromolecules* **2012**, *45* (1), 283−291.

(13) Wanakule, N. S.; Virgili, J. M.; Teran, A. A.; Wang, Z.-G.; Balsara, N. P. Thermodynamic Properties of Block Copolymer Electrolytes Containing Imidazolium and Lithium Salts. *Macromolecules* **2010**, *43* (19), 8282−8289.

(14) Nakamura, I.; Balsara, N. P.; Wang, Z. G. Thermodynamics of Ion-Containing Polymer Blends and Block Copolymers. *Phys. Rev. Lett.* **2011**, *107* (19), 5.

(15) Nakamura, I.; Wang, Z.-G. Salt-Doped Block Copolymers: Ion Distribution, Domain Spacing and Effective chi Parameter. *Soft Matter* **2012**, *8* (36), 9356−9367.

(16) Wang, Z. G. Effects of Ion Solvation on the Miscibility of Binary Polymer Blends. *J. Phys. Chem. B* **2008**, *112* (50), 16205−16213.

(17) Hadjichristidis, N.; Iatrou, H.; Pispas, S.; Pitsikalis, M. Anionic Polymerization: High Vacuum Techniques. *J. Polym. Sci., Part A: Polym. Chem.* **2000**, *38* (18), 3211−3234.

(18) Quirk, R. P.; Kim, J.; Kausch, C.; Chun, M. S. Butyllithium-Initiated Anionic Synthesis of Well-Defined Poly(styrene-block-ethylene oxide) Block Copolymers with Potassium Salt Additives. *Polym. Int.* **1996**, *39* (1), 3−10.

(19) Mark, J. E., *Physical Properties of Polymers Handbook*, 2nd ed.; Springer: Philadelphia, PA, 2007.

(20) Yuan, R.; Teran, A. A.; Gurevitch, I.; Mullin, S. A.; Wanakule, N. S.; Balsara, N. P. Ionic Conductivity of Low Molecular Weight Block Copolymer Electrolytes. *Macromolecules* **2013**, *46* (3), 914−921.

(21) Gomez, E. D.; Panday, A.; Feng, E. H.; Chen, V.; Stone, G. M.; Minor, A. M.; Kisielowski, C.; Downing, K. H.; Borodin, O.; Smith, G. D.; Balsara, N. P. Effect of Ion Distribution on Conductivity of Block Copolymer Electrolytes. *Nano Lett.* **2009**, *9* (3), 1212−1216.

(22) Ilavsky, J., Nika: Software for Two-Dimensional Data Reduction. *J. Appl. Crystallogr.* **2012**, *45*.

(23) Leibler, L. Theory of Microphase Separation in Block Co-Polymers. *Macromolecules* **1980**, *13* (6), 1602−1617.

(24) Khandpur, A. K.; Forster, S.; Bates, F. S.; Hamley, I. W.; Ryan, A. J.; Bras, W.; Almdal, K.; Mortensen, K. Polyisoprene−Polystyrene Diblock Copolymer Phase Diagram near the Order−Disorder Transition. *Macromolecules* **1995**, *28* (26), 8796−8806.

(25) Floudas, G.; Vazaiou, B.; Schipper, F.; Ulrich, R.; Wiesner, U.; Iatrou, H.; Hadjichristidis, N. Poly(ethylene oxide-*b*-isoprene) Diblock Copolymer Phase Diagram. *Macromolecules* **2001**, *34* (9), 2947−2957.
(26) Wang, J. Y.; Chen, W.; Russell, T. P. Ion-Complexation-Induced Changes in the Interaction Parameter and the Chain Conformation of PS-*b*-PMMA Copolymers. *Macromolecules* **2008**, *41* (13), 4904−4907.
(27) Wen, S. J.; Richardson, T. J.; Ghantous, D. I.; Striebel, K. A.; Ross, P. N.; Cairns, E. J. FTIR Characterization of PEO + $LiN(CF_3SO_2)(2)$ Electrolytes. *J. Electroanal. Chem.* **1996**, *408* (1−2), 113−118.
(28) Schweizer, K. S.; Curro, J. G. Integral-Equation Theory of the Structure and Thermodynamics of Polymer Blends. *J. Chem. Phys.* **1989**, *91* (8), 5059−5081.
(29) Schweizer, K. S. Analytic Rism Theory of Polymer Alloys—Molecular Closure Predictions for Structurally Symmetrical Blends. *Macromolecules* **1993**, *26* (22), 6033−6049.
(30) Sariban, A.; Binder, K. Critical Properties of The Flory−Huggins Lattice Model of Polymer Mixtures. *J. Chem. Phys.* **1987**, *86* (10), 5859−5873.
(31) Fried, H.; Binder, K. The Microphase Separation Transition in Symmetrical Diblock Copolymer Melts—A Monte-Carlo Study. *J. Chem. Phys.* **1991**, *94* (12), 8349−8366.
(32) Binder, K.; Fried, H. Asymmetric Block-Copolymer Melts Near the Microphase Separation Transition—A Monte-Carlo Simulation. *Macromolecules* **1993**, *26* (25), 6878−6883.
(33) Bates, F. S.; Muthukumar, M.; Wignall, G. D.; Fetters, L. J. Thermodynamics of Isotopic Polymer Mixtures—Significance of Local Structural Symmetry. *J. Chem. Phys.* **1988**, *89* (1), 535−544.
(34) Maranas, J. K.; Kumar, S. K.; Debenedetti, P. G.; Graessley, W. W.; Mondello, M.; Grest, G. S. Liquid Structure, Thermodynamics, and Mixing Behavior of Saturated Hydrocarbon Polymers. 2. Pair Distribution Functions and the Regularity of Mixing. *Macromolecules* **1998**, *31* (20), 6998−7002.
(35) Maranas, J. K.; Mondello, M.; Grest, G. S.; Kumar, S. K.; Debenedetti, P. G.; Graessley, W. W. Liquid Structure, Thermodynamics, and Mixing Behavior of Saturated Hydrocarbon Polymers. 1. Cohesive Energy Density and Internal Pressure. *Macromolecules* **1998**, *31* (20), 6991−6997.
(36) Luettmer-Strathmann, J.; Lipson, J. E. G. Miscibility of Polyolefin Blends. *Macromolecules* **1999**, *32* (4), 1093−1102.
(37) Muller, M.; Binder, K. Computer-Simulation of Asymmetric Polymer Mixtures. *Macromolecules* **1995**, *28* (6), 1825−1834.
(38) Wang, Z. G. Concentration Fluctuation in Binary Polymer Blends: Chi Parameter, Spinodal and Ginzburg Criterion. *J. Chem. Phys.* **2002**, *117* (1), 481−500.
(39) Wittmer, J. P.; Beckrich, P.; Meyer, H.; Cavallo, A.; Johner, A.; Baschnagel, J., Intramolecular Long-Range Correlations in Polymer Melts: The Segmental Size Distribution and its Moments. *Phys. Rev. E: Stat., Nonlinear, Soft Matter Phys.* **2007**, *76* (1).
(40) Morse, D. C.; Chung, J. K., On the Chain Length Dependence of local Correlations in Polymer Melts and a Perturbation Theory of Symmetric Polymer Blends. *J. Chem. Phys.* **2009**, *130* (22).
(41) Jian, Q.; Morse, D. C. Renormalized One-loop Theory of Correlations in Polymer Blends. *J. Chem. Phys.* **2009**, *130* (22), 224902 (15 pp.)−224902 (15 pp.).
(42) Yethiraj, A.; Schweizer, K. S. Self-Consistent Polymer Integral-Equation Theory—Comparisons with Monte-Carlo Simulations and Alternative Closure Approximations. *J. Chem. Phys.* **1992**, *97* (2), 1455−1464.